Mon. Not. R. Astron. Soc. **000**, 1–10 (2016) Printed 21 July 2016 (MN LATEX style file v2.2)

Upper limits to the number of Oort Cloud Objects based on serendipitous occultation events search in X-rays

Hsiang-Kuang Chang[1,2⋆], Chih-Yuan Liu[1], and Jie-Rou Shang[1]
[1] *Institute of Astronomy, National Tsing Hua University, Hsinchu 30013, Taiwan*
[2] *Department of Physics, National Tsing Hua University, Hsinchu 30013, Taiwan*

arXiv:1607.05797v1 [astro-ph.EP] 20 Jul 2016

Accepted 2016 July 19. Received 2016 July 17; in original form 2016 May 30

ABSTRACT

Using all the RXTE archival data of Sco X-1 and GX 5-1, which amount to about 1.6 mega seconds in total, we searched for possible occultation events caused by Oort Cloud Objects. The detection efficiency of our searching approach was studied with simulation. Our search is sensitive to object size of about 300 m in the inner Oort Cloud, taking 4000 AU as a representative distance, and of 900 m in the outer Oort Cloud, taking 36000 AU as the representative distance. No occultation events were found in the 1.6 Ms data. We derived upper limits to the number of Oort Cloud Objects, which are about three orders of magnitude higher than the highest theoretical estimates in the literature for the inner Oort Cloud, and about six orders higher for the outer Oort Cloud. Although these upper limits are not constraining enough, they are the first obtained observationally, without making any model assumptions about comet injection. They also provide guidance to such serendipitous occultation event search in the future.

Key words: occultations – Kuiper Belt: general – Oort Cloud – stars: neutron – X-rays: binaries.

1 INTRODUCTION

Existence of the Oort Cloud, which was proposed 66 years ago (Oort 1950), has not yet been directly confirmed, except for the discovery of Sedna (Brown, Trujillo & Rabinowitz 2004), 2012 VP_{113} (Trujillo & Sheppard 2014) and three other objects (Chen et al. 2013; Brasser & Schwamb 2015), which are considered to be inner Oort Coloud Objects. The population properties of Oort Cloud Objects are not yet clear either, such as their total number and size distribution. The knowledge of these properties is important to our understanding of the origin and evolution of the Oort Cloud.

Oort Cloud Objects are usually thought to form in the outer planetary region and to be ejected to a distance far away from the sun by giant outer planets (for brief reviews, see, e.g., Dones et al. (2004a); Rickman (2014); Dones et al. (2015)). Galactic tides, star/giant-molecular-cloud encounters, and planetary perturbations all affect the formation and evolution of the Oort Cloud as well as the injection of Oort Cloud Objects into the inner solar system. With a proper injection model and observed flux of long-period comets, one can in principle infer the number of objects in the Oort Cloud. This has been being the effort made by many authors with various physical considerations. In Duncan et al. (1987) it was found, by direct numerical integration, that the Oort Cloud has a sharp inner edge at about 3000 AU and the number density of Oort Cloud Objects falls steeply outwards, roughly as $r^{-3.5}$. The Oort Cloud is therefore centrally condensed, with roughly 5 times more objects in the inner Oort Cloud ($a < 20,000$ AU) than in the classical outer Oort Cloud. In a later study, Weissman (1996) estimated that there are 10^{12} objects of diameter larger than 2.3 km in the outer Oort Cloud ($a > 20,000$ AU). The inner Oort Cloud was originally proposed by Hills (1981). Kaib & Quinn (2009) demonstrated that a significant fraction of long-period comets in fact come from the inner Oort Cloud before their migration into the outer Oort Cloud due to planetary perturbation. It was estimated in Kaib & Quinn (2009) that there could be $\sim 10^{12}$ objects in the inner Oort Cloud (3000 AU $< a <$ 20,000 AU). Some estimates yielding smaller numbers of objects in the outer Oort Cloud, about 2×10^{11} – 5×10^{11}, were reported in Heisler (1990); Dones et al. (2004b); Brasser & Morbidelli (2013).

Direct observation of objects in the Oort Cloud region is extremely difficult. Their existence, however, in addition to being inferred from observations of long-period comets, may also be explored by occultation events that they cause to distant background stars. Such an approach, looking for serendipitous occultation events from a vast amount

⋆ E-mail: hkchang@phys.nthu.edu.tw

© 2016 RAS

of data, has been being employed to study the size distribution of small Kuiper Belt Objects (KBOs) down to sub-kilometer size using optical data (Roques et al. 2006; Bickerton, Kavelaars & Welch 2008; Schlichting et al. 2012; Zhang et al. 2013; Liu et al. 2015) and even to decameter size using X-ray observations (Chang, Liu & Chen 2013). It has also been applied to estimating upper limits to the number of small objects at distances between 100 and 1000 AU with data accumulated by the TAOS project (Wang et al. 2009).

In this paper we report the result of our effort to extend the work of serendipitous KBO occultation search in X-rays to the regime relevant to possible occultation events caused by Oort Cloud Objects. Our conclusion is that in all the RXTE archival data of Sco X-1 and GX 5-1, 1.6 mega seconds in total, no such events were found. The derived upper limits to the number of inner and outer Oort Cloud Objects are about three orders of magnitude higher than the highest theoretical estimates in the literature for the inner, and about six orders higher for the outer, respectively. Although these upper limits are not constraining enough, they are the first obtained observationally, without making any model assumptions about comet injection. They also provide guidance to observations in the future. At the end of this paper, we discuss the possibility of using ASTROSAT (Singh et al. 2014), Athena (a future ESA X-ray space mission (Ayre et al. 2015)) and LOFT (a proposed mission (Zane et al. 2014)) to conduct such a search to study the size distribution of Oort Cloud Objects and KBOs.

2 SEARCHING FOR OCCULTATION EVENTS IN X-RAYS CAUSED BY SMALL OORT CLOUD OBJECTS

It is clear that small Trans-Neptunian Objects (TNOs, referred to all the solar system objects beyond Neptune, including KBOs and Oort Cloud Objects) cannot be observed directly. Roughly speaking, an object of V-band magnitude 30 is about 10 km in diameter if it is at 50 AU, and about 1000 km at 500 AU (see e.g. Roques et al. (2009)). Serendipitous occultation search is so far the only way to 'observe' objects smaller than that. Optical search has the advantage of monitoring many stars at the same time, while in X-rays even smaller objects can be probed because of less diffraction in the occultation light curve. To date, such search is focused on pinning down the size distribution of small KBOs (Roques et al. 2006; Bickerton, Kavelaars & Welch 2008; Schlichting et al. 2012; Chang, Liu & Chen 2013; Zhang et al. 2013; Liu et al. 2015), which are located mainly between 30 and 50 AU. We now extend this effort to the Oort Cloud, using X-ray data.

To perform such serendipitous occultation search in X-rays, the background X-ray source must be bright enough or the detector effective area needs to be large enough so that there are enough detected photons to allow statistically significant determination of occurrence of occultation events and, if possible, to allow meaningful determination of some information from fitting the occultation light curve with diffraction patterns of given parameters. The Proportional Counter Array (PCA) on board RXTE has the largest effective area among all the astronomical X-ray instruments until the launch of ASTROSAT in 2015 and Sco X-1 is the brightest X-ray source in the sky other than the Sun. The PCA-observed spectrum of Sco X-1 peaks at 4 keV, for which the Fresnel scale is 30 m at 40 AU. The shadow of KBOs of that Fresnel-scale size will sweep over the Earth in milliseconds. The RXTE/PCA count rate of Sco X-1 is rouhly 10^5 cps, which is about enough for examining possible events at millisecond time scales. That is why in earlier attempts (Chang et al. 2006, 2007; Chang, Liu & Chen 2011, 2013) only RXTE data of Sco X-1 was employed to look for occultation events caused by KBOs down to decameter size. Other background sources are all too dim for such millisecond-time-scale search (cf. Table 3 in Chang, Liu & Chen (2013)).

Sco X-1		GX 5-1	
Count rates (cps)	Data	Count rates (cps)	Data
4,000 - 20,000	50.6 ks	4,000 - 6,000	4.9 ks
20,000 - 40,000	134.3 ks	6,000 - 8,000	203.1 ks
40,000 - 60,000	154.7 ks	8,000 - 10,000	115.0 ks
60,000 - 80,000	282.2 ks	10,000 - 12,000	115.7 ks
80,000 - 100,000	226.2 ks	12,000 - 14,000	73.9 ks
100,000 - 120,000	127.8 ks	14,000 - 16,000	72.2 ks
120,000 - 140,000	13.0 ks	16,000 - 18,000	2.5 ks
Total	988.9 ks	Total	587.2 ks

Table 1. The count-rate distribution of the RXTE/PCA Sco X-1 and GX 5-1 data employed in this work. Total data volume is 1.6 Ms. The average count rate for Sco X-1 is about 80000 cps and for GX 5-1 about 8000 cps.

For Oort Cloud Objects, we take 4000 AU and 36000 AU as two representative distances for the inner and outer cloud respectively. The corresponding Fresnel scales are 300 m and 900 m and the relevant time scale is then tens of milliseconds. We note that, although shadow size decreases with decreasing object size, its diameter will asymptotically approach 3.4 Fresnel scales for small objects (Nihei et al. 2007), assuming the background source is a point one. We therefore conducted the search with light curves binned at 10, 30, 60, 90 and 180 ms. With such bin sizes, we added another source, GX 5-1, which is the second brightest according to RXTE/ASM count rates (cf. Table 3 in Chang, Liu & Chen (2013)), to conduct this search. Their count rates are of considerable variation, depending on observation conditions and the intrinsic variability of the sources. We examined all of their RXTE/PCA data, collected data of adequate data modes, and selected data of average count rates in a pointing larger than 4000 cps for our search. The count rate distribution of the data we used is shown in Table 1.

Our searching algorithm is the same as the one we used before (e.g. Chang et al. (2007); Chang, Liu & Chen (2011)), but with data binned at a larger time scale. Briefly speaking, we examine their light curves binned at 10, 30, 60, 90 and 180 ms to look for bins with statistically significant photon-count drop. We assign to each bin a deviation score, which is the difference between the photon count number of that bin and the average count number per bin in an 8-sec

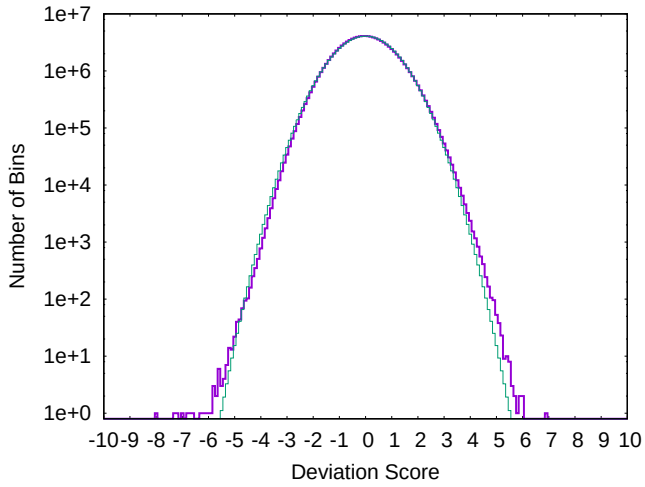

Figure 1. The deviation distribution of all the light curves from the 1.6-Ms data binned at 10 ms (thick purple histogram). A Gaussian distribution is plotted for comparison (thin green histogram). The data, because of its Poisson nature, is not expected to follow the Gaussion distribution strictly. The six events with deviation scores below -6.5 are apparently outliers in this distribution. Another event with a deviation score of -11.8 is not shown here. More details of these events are discussed in the text and shown in Figure 2. The event at $+6.9\sigma$ is statistically significant and will be further studied, but it is not relevant to the subject of this paper.

Event	Epoch (MJD)	RXTE ObsId	Significance
1	50228.94786301	10056-01-02-00	-7.3σ
2	50820.70967736	30036-01-01-000	-8.0σ
3	52413.98833994	70015-01-01-01	-7.4σ
4	54333.91603852	93067-01-08-00	-11.8σ
5	54765.73618319	93067-01-28-00	-6.7σ
6	55699.14184696	93067-04-20-00	-6.6σ
7	55928.58787662	96443-03-01-05	-7.0σ

Table 2. Epochs of the seven events found in the 10-ms light curves.

running window in units of the standard deviation in that 8-sec window. To judge whether a dip event is consistent with random fluctation, we compare the deviation distribution of all bins in a search at a certain bin size with a Gaussian distribution. In all of our search, we found seven bins with deviation stronger than -6.5σ. All of them are found in the case of 10-ms bin size, whose deviation distribution is shown in Figure 1. These seven bins are apparently outliers in that deviation distribution. The level at -6.5σ corresponds roughly to a random probability of 10^{-3} if a Gaussion distribution is assumed and the total number of bins is taken into account.

More details of these seven events are shown in Table 2 and Figure 2. Among these seven events, Events 4, 5 and 6 are associated with events found at smaller bin size reported in Chang, Liu & Chen (2013) that come together with the so-called Very Large Events (VLEs). RXTE's VLEs are events that deposit more than 100 keV into an individual anode in a Proportional Counter Unit (PCU). RXTE/PCA consists of five identical PCUs. An instrument dead-time of 50 μs is set for each VLE during RXTE observations of Sco X-1. VLEs are produced by high energy photons or particles. In order to clarify whether VLEs cause the dip events reported in Chang et al. (2006, 2007), a special data mode was designed for the RXTE observation proposal 93067 to record each individual VLE with μs resolution and information of all the triggerred anodes. In usual housekeeping data, VLEs are recorded only with its total number in a 125-ms bin. It was found that all the millisecond dip events, except for one, are associted with VLEs. They are considered instrumental, although not expected at the beginning with a 50-μs dead time. As can be seen in Figure 2, these three events all have an asymmetric profile in their 2-ms light curves. They also all have some excess in the 'Remaining' counts, which are all the events except for good events, VLEs and propane events. Good events are those that trigger only one xenon anode. The propane event is the one that triggers only the propane layer, which is designed to distinguish events caused by soft electrons from those by X-rays. The remaining counts contain many multiple-anode events, which are usually treated as particle background. Excess in the 'Remaining' counts is indication of instrumental effects. The other four events, that is, Events 1, 2, 3, and 7 are all either with asymmetric profiles in thier 2-ms light curves or with some 'Remaining' count excess. Besides, all these seven events are found in Sco X-1's light curves. None is in GX 5-1's. These events all show a deep drop in the light curve, but not down to zero, in a certain 2-ms bin, and then gradually 'recover' back to normal. Such a dip, when binned at 10 ms, has only a modest equivalent depth. For GX 5-1, with a typical count number of 80 in a 10-ms bin, such a dip will not have a deviation score as large as -6.5, because of its small count number in one bin. We therefore conclude that they are all instrumental. No dip events were found in the 1.6 Ms data with light curves binned at 10-, 30-, 60-, 90- and 180-ms.

3 RXTE DETECTION EFFICIENCY FOR OCCULTATIONS CAUSED BY SMALL OORT CLOUD OBJECTS

To derive the size distribution from detected event rates, we need to know the detection efficiency of the searching approach. In Chang, Liu & Chen (2013), it was studied for the case of detecting KBO occultation events with RXTE data of Sco X-1. In this paper we do the same but for the case of detecting Oort Cloud Object occultation events, which involves different time scales in the searching algorithm and different shadow diffraction patterns because of the possibly non-negligible size of the X-ray emitting region in Sco X-1 and GX 5-1 as projected at the distance of the Oort Cloud.

The detection efficiency, η, depends on the 'shadow size' that one adopts, detector count rate of the background source, relative speed, and the searching algorithm. In the geometric optics regime the shadow size is simply the diameter D of the occulting body, if the background star can be well approximated as a point source. If the size of the background star is not negligible, the full shadow size, including umbra and penumbra, will be $D + D_*$, where D_* is the projected diameter of the background star at the distance of the

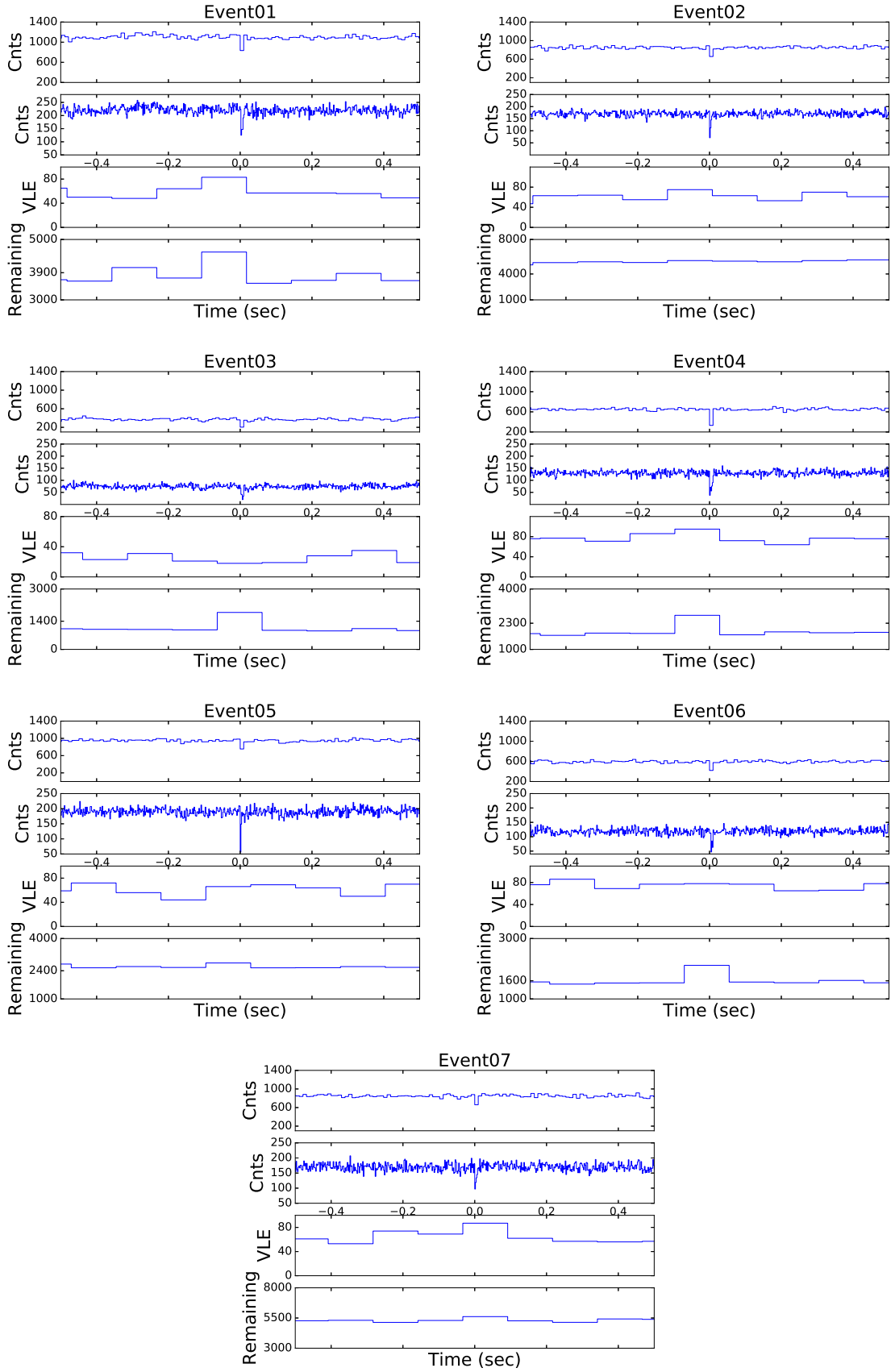

Figure 2. Light curves of the seven dip events in a 1-s window. Shown here for each event, from top to bottom, are the light curves binned at 10 ms and 2 ms, and of the 'VLE' and 'Remaining' counts, which are only available with 125-ms resolution in the RXTE/PCA housekeeping data. See the text for the explanation of 'VLE' and 'Remaining' counts.

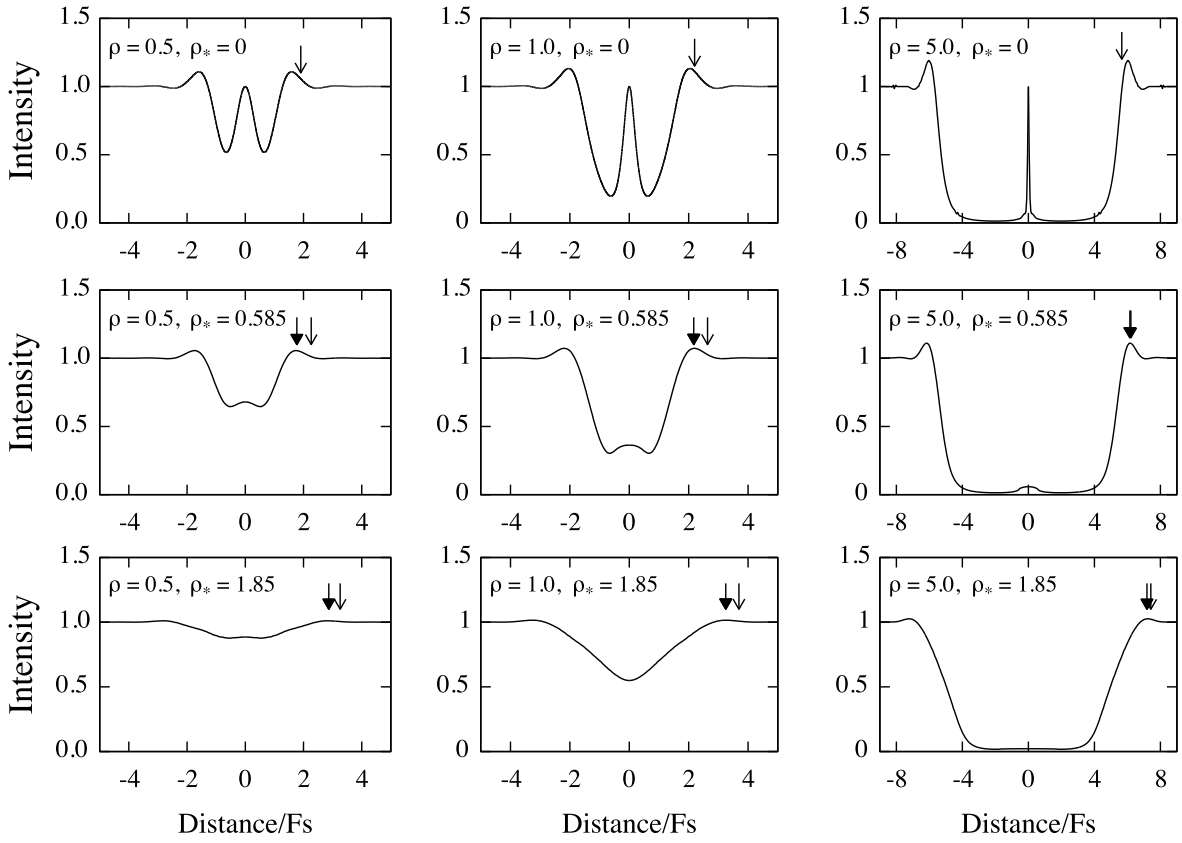

Figure 3. Some example diffraction patterns of central-crossing events for different sizes of the occulting body and the background source. Shown here are that for occulting body radius 0.5 Fs (panels in the left column), 1.0 Fs (the middle column) and 5.0 Fs (the right column). The panels in the top row are for background sources being a point source, in the middle row for radius 0.585 Fs, and in the bottom row radius 1.85 Fs. Thick arrow symbols indicate the shadow boundary we adopt, which is at the fring peak. Thin arrow symbols indicate the shadow boundary as given by Eq.(4) in Nihei et al. (2007) for extended background sources. In the middle right panel, the two arrows almost coincident. In the top row, for a point-like background source ($\rho_* = 0$), the thin arrows indicate the shadow boundary as described by $\Omega = 2(\sqrt{3}^{3/2} + \rho^{3/2})^{2/3}$ (Nihei et al. 2007). We adopt this in our simulation for the case of point-like background sources. A typical RXTE/PCA observed Sco X-1 spectrum is used for the computation.

occulting body. When diffraction matters, it is larger and not well defined. For a point-like background source, taking the fringe peak as the shadow boundary, it was found that (Nihei et al. 2007) the relation between the shadow size Ω and the occulting body radius ρ can be approximatedly described as $\Omega = 2(\sqrt{3}^{3/2} + \rho^{3/2})^{2/3}$, in which both Ω and ρ are those in units of Fresnel scale. For extended background sources, it was suggested to be $\Omega = 2(\sqrt{3}^{3/2} + \rho^{3/2})^{2/3} + 2\rho_*$ (Eq.(4) in Nihei et al. (2007)), where ρ_* is the projected radius of the background star at the distance of the occulting body.

The size of the X-ray emitting region in Low Mass X-ray Binaries, such as Sco X-1 and GX 5-1, is not yet well determined. It could range from about 50 km to 50000 km, depending on different models (e.g., see Barnard, Church & Balucinska-Church (2003); Bradshaw, Geldzahler & Fomalont (2003); Revnivtsev et al. (2014); Hynes et al. (2016) for Sco X-1, and Jackson, Church & Balucińska-Church (2009); Sriram, Choi & Rao (2012) for GX 5-1). For the largest end, 50000 km, the projected size at 40, 4000 and 36000 AU for Sco X-1, whose distance is 2.8 kpc, is roughly 3.6, 360 and 3240 m respectively, which is about 0.12, 1.2, and 3.6 Fresnel scale. The Fresnel scale (Fs hereafter) is defined as $\sqrt{\lambda d/2}$, where λ is the wavelength and d is the distance. It is about 30 m for $d = 40$ AU and $\lambda = 0.3$ nm (4 keV; most photons in the RXTE data of Sco X-1 and GX 5-1 are at about this energy). The distance to GX 5-1 is not quite certain. From column density estimate, it is about 9 kpc (Christian & Swank 1997). In the Oort Cloud region, therefore, we should consider the possibility of an extended background source.

We computed shadow patterns of Fresnel-scale sized TNOs for three background-target sizes: a point source, 0.585 Fs radius, and 1.85 Fs radius, with a typical RXTE-observed Sco X-1 spectrum. Example shadow patterns of TNOs with 0.5 Fs, 1.0 Fs, and 5.0 Fs radius are shown in Figure 3, in which the shadow-size range we adopt is indicated, which uses the diffraction fringe peak as the boundary of the shadow. The numerically computed shadow size as a function of TNO size is plotted in Figure 4. This shadow size is what we use in our simulation for determining detection efficiency. In practice we use a polynomial fit to describe it. We note that the expression in Nihei et al. (2007) (Eq.(4))

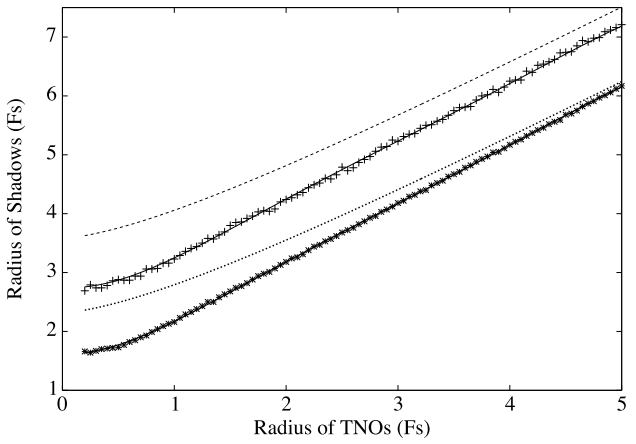

Figure 4. The shadow radius as a function of TNO radius for extended background sources. Shown with asterisk symbols (the lower curve) is the case for the extended source radius being 0.585 Fs, and with cross symbols (the upper curve) for radius 1.85 Fs. A polynomial fit, which is used in our detection efficiency simulation, is shown with solid lines passing through those symbols. Dotted and Dashed lines are those obtained from Eq.(4) in Nihei et al. (2007) for the cases of 0.585 Fs and 1.85 Fs, respectively.

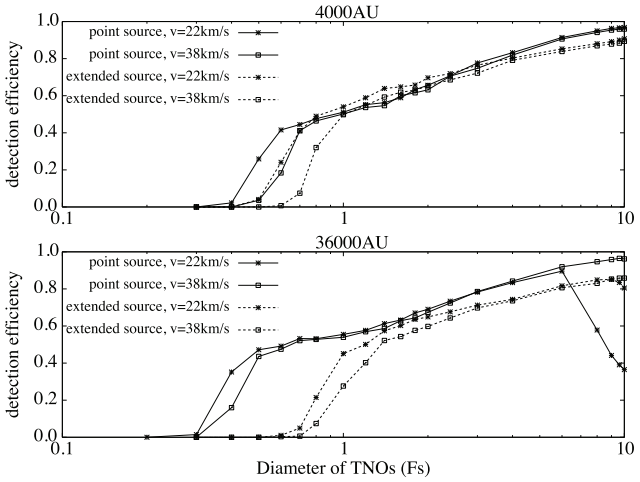

Figure 5. The detection efficiency as a function of TNO diameter. Solid lines are for the background source being a point one and dashed lines for extended background sources. In the upper panel the diameter of the extended background source is 1.2 Fs (360 m), corresponding to 50000 km at 2.8 kpc projected at 4000 AU, and in the lower panel it is 3.6 Fs (3240 m), corresponding to that at 36000 AU. The lines with asterisk symbols are for the relative speed being 22 km/s and those with open squares for 38 km/s. The drop of the solid line with asterisk symbols close to 10 Fs in the lower panel is discussed in the text.

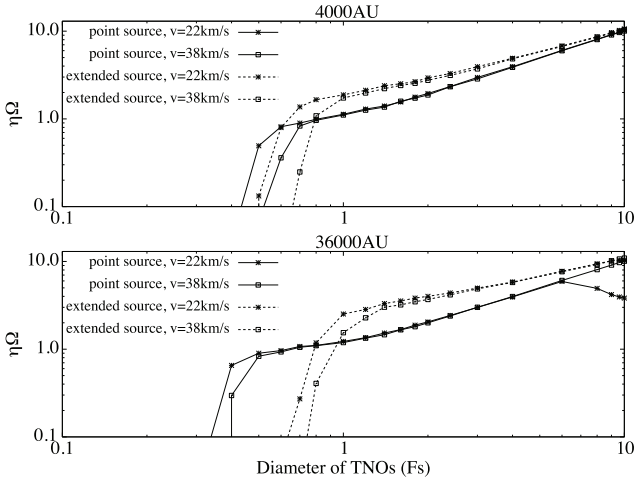

Figure 6. The product of detection efficiency and shadow diameter as a function of TNO diameter. Figure legend is the same as that in Figure 5. The shadow diameter is the one we adopt as shown in Figure 4.

gives a shadow size larger than that defined by the diffraction fringe peaks, particularly for smaller occulting bodies. It is also shown in Figure 4.

When estimating the detection efficiency with simulations, as detailed below, we randomly pick an impact parameter β, ranging from zero to the shadow radius, in each simulation. The impact parameter β is the distance between the center of the background star and that of the occulting body. In principle one may consider a larger range for the impact parameter, but in that case the detection efficiency will be lower and more efforts are required to obtain a statistically stable solution. What really matters in deriving the size distribution (see Eq.(4) is the product of the detection efficiency and the shadow size, the latter of which is represented by the impact-parameter range in the simulation. In this sense, the shadow size expression for extended background sources as suggested in Nihei et al. (2007) may also be used. The product $\eta\Omega$ should have the same value for different choices of Ω, which defines the impact-parameter range, if they are all chosen to be large enough.

In the following we present simulation results of detection efficiency for cases of assuming the occulting body being at 4000 AU (inner Oort Cloud) and 36000 AU (outer Oort Cloud). We used typical RXTE/PCA-observed spectra of Sco X-1 and GX 5-1, which both peak at about 4 keV, as the input spectra when computing the diffraction pattern. The count rate is set at 80000 cps for Sco X-1 and at 8000 cps for GX 5-1. In both the cases of inner and outer Oort Cloud, we further distinguish the possibility of treating the background sources as a point-like source or as an extended source. As discussed above, the X-ray emitting region in these sources is not well determined. It is model dependent and could range from about 50 km to 50000 km. Sco X-1 is at 2.8 kpc away. A scale of 50 km at 2.8 kpc corresponds to 0.36 m at 4000 AU and 3.2 m at 36000 AU. The Fresnel scale is 300 m at 4000 AU and 900 m at 36000 AU. It is therefore still a good approximation to treat Sco X-1 as a point-like source if its X-ray emitting region is close to 50 km. The same also applies to GX 5-1, whose distance is likely about 9 kpc. On the other hand, if it is 3 orders larger, that is, close to 50000 km, it will be 1.2 Fresnel scale at 4000 AU and 3.6 Fresnel scales at 36000 AU for Sco X-1. For Gx 5-1 it would be three times smaller if we still assume a 50000-km X-ray emitting region. It is, however, not really meaningful to distinguish the size of the possible extended regions between Sco X-1 and GX 5-1, because that is very uncertain. We therefore use those values for the cases of 'ex-

tended sources' in our simulation for both Sco X-1 and GX 5-1.

In each simulation with a given relative speed and the occulting body size, we performed 10000 runs of event search in the simulated light curve. In each run, we randomly pick the impact parameter β in the range from zero to the shadow radius (see discussion at the beginning of this section) and the epoch of the implanted occultation event. We conducted the same algorithm as we used in searching for dip events with real data binned at different bin size. The threshold of detection is set at -6.5σ. Figure 5 shows the results of the detection efficiency for the case of Sco X-1. The actuall relative speed between the occulting body and the RXTE satellite for each possible event depends on the velocity of RXTE in the solar system at the event epoch and that of the occulting body. For very distant objects, the latter can be neglected. Since RXTE observations of Sco X-1 were conducted more intensively when Sco X-1 is close to opposition and the RXTE orbital speed relative to the Earth is about 7.8 km/s, we consider relative speeds being 30 ± 8 km/s in our simulation. Exact relative speed can be found for specific candidate occultation events (Chang, Liu & Chen 2011). There are some points to note: First, roughly speaking, the detection efficiency gets larger than 50% for occulting TNO size (diameter) larger than one Fresnel scale for all cases. Second, even for TNOs as large as of 10-Fs diameter, the detection efficiency is still noticeably below 100%. This is because of those cases with impact parameters close to the shadow radius. It is more apparent when the background target is extended, since the corresponding diffraction pattern has a more gradual transition boundary, and therefore there is a shallower shadow for a larger range of large impact parameters; see the right panels of Figure 3 and compare the boundary transition from the top panel to the bottom. Third, in the lower panel of Figure 5, we see an obvious drop of the detection efficiency for the point-source lower-speed case close to 10-Fs diameter. This is because the shadow duration, which is about 450 ms for a central-crossing event when the relative speed is 22 km/s, is much larger than the bin size used in the search, the largest of which is 180 ms. The shadow causes an overestimate of the standard deviation in the search running window and suppresses the chance of detection. For such cases, the more gradual transition boundary caused by an extended background target actually reduces that overestimate and the suppression is therefore weaker, as shown for the lower-speed extended-source case in the lower panel of Figure 5. Fourth, the results for GX 5-1 are similar to that of Sco X-1, except that the 50% detection efficiency occurs at an TNO diameter of about 2 Fs, rather than 1 Fs. This is of course due to the lower count rate.

As discussed earlier and also shown in Eq.(4), when estimating the event rate, what matters is the product $\eta\Omega$ as a function of TNO diameter D, which is plotted in Figure 6. One can see that $\eta\Omega$ is close to D/Fs for D larger than about 1 Fs. Based on all these results, we consider one Fresnel scale as an appropriate smallest size that our approach can probe. In the next section we further approximate $\eta\Omega$ with D/Fs for D larger than 1 Fs. This is somewhat underestimated, and therefore the inferred upper limit is overestimated a little bit.

4 UPPER LIMITS TO THE NUMBER OF OORT CLOUD OBJECTS

To describe the size distribution of a certain population, such as MBAs, KBOs or Oort Cloud Objects, one often uses the accumulated number of objects larger than a certain size per unit sky area, $n_{D>D_1}$, defined as

$$n_{D>D_1} = \int_{\infty}^{D_1} \frac{\mathrm{d}n}{\mathrm{d}D}\,\mathrm{d}D \quad , \tag{1}$$

where $\frac{\mathrm{d}n}{\mathrm{d}D}$ is the differential size distribution. In collisional equilibrium, one expects to have (O'Brien & Greenberg 2003) $\frac{\mathrm{d}n}{\mathrm{d}D} \propto D^{-q}$ and $q = \frac{7+p/3}{2+p/3}$, where p is the power index of the strength-size relation. In the so-called strength-scaled regime (in contrast to the gravity-scaled regime for larger bodies), p is negative. It has been found that the size distribution of MBAs has a wavy shape, or, approximately, the power index q takes different values in different size ranges (see, e.g., Yoshida & Nakamura (2007)). Similar behavior was also tentatively found for KBOs (see, e.g., Liu et al. (2015)). Within a certain size range in which a constant power index q is a good approximation, the accumulated number density and the differential number density is related as

$$n_{D_2>D>D_1} = \left(\frac{\mathrm{d}n}{\mathrm{d}\log D}\right)_{D_0} \frac{1}{\ln 10}\frac{1}{-q+1}((\frac{D_1}{D_0})^{-q+1} - (\frac{D_2}{D_0})^{-q+1}), \tag{2}$$

where the definition

$$\frac{\mathrm{d}n}{\mathrm{d}D} = \left(\frac{\mathrm{d}n}{\mathrm{d}D}\right)_{D_0}\left(\frac{D}{D_0}\right)^{-q} \tag{3}$$

is adopted.

The event rate of serendipitous occultation caused by TNOs of diameter D in the range of $D_2 > D > D_1$, for one background source, can be estimated as

$$\frac{N}{T} = \int_{D_2}^{D_1} \frac{\mathrm{d}n}{\mathrm{d}D}\frac{(\eta\Omega\,\mathrm{Fs})\,v}{d^2}\,\mathrm{d}D\,\left(\frac{180}{\pi}\right)^2 \quad , \tag{4}$$

where N is the number of events, T the total observing time, n in units of number per square degree, $\eta\Omega$ is the product of detection efficiency and the shadow size as described in the previous section, v the relative speed between TNO and the observer, and d the distance. In this paper we approximate $\eta\Omega$ with D/Fs for D larger than one Fresnel scale; more details are described in the previous section, the study of detection efficiency. We do not have detailed information about v and d as functions of D. Typical, or representative, values are assumed to estimate the event rate.

Since we do not have any knowledge about the size distribution of Oort Cloud Objects, let us first assume a constant power index q for objects with diameter larger than one Fresnel scale, denoted as D_1 below, which is clsoe to the smallest size to which our search is sensible. The event rate is then

$$\frac{N}{T} = \left(\frac{\mathrm{d}n}{\mathrm{d}\log D}\right)_{D_0}\frac{1}{\ln 10}\frac{1}{-q+2}((\frac{D_1}{D_0})^{-q+2} - (\frac{D_2}{D_0})^{-q+2})\frac{D_0 v}{d^2}(\frac{180}{\pi})^2\,. \tag{5}$$

Considering $D_2 \gg D_1$ and $q > 2$, we then have, taking $D_0 = D_1$,

$$n_{D>D_1} = \frac{N}{T}\left(\frac{-q+2}{-q+1}\right)\frac{d^2}{D_1 v}(\frac{\pi}{180})^2 \quad . \tag{6}$$

Since there is no detection in the 1.6 Ms RXTE data that we employed, we estimate the upper limit to the size distribution at 95% confidence level with $N = 3$. The Fresnel scale at 4000 AU and 36000 AU, for 4 keV photons, is about 300 m and 900 m respectively. Taking $v = 30$ km/s and $q = 3.5$, we then have, for the inner Oort Cloud

$$n_{D>300m} < 1.4 \times 10^{13}\,\mathrm{deg}^{-2} \quad , \tag{7}$$

and for the outer Oort Cloud

$$n_{D>900m} < 3.6 \times 10^{14}\,\mathrm{deg}^{-2} \quad . \tag{8}$$

Assuming an isotropic distribution, the total number is

$$N_{D>300m} < 5.4 \times 10^{17} \quad \text{for the inner Oort Cloud} \quad , \tag{9}$$

and

$$N_{D>900m} < 1.5 \times 10^{19} \quad \text{for the outer Oort Cloud} \quad . \tag{10}$$

These upper limits are way above earlier theoretical estimates in the literature. If we consider the estimate that there are about 10^{12} comets of diameter larger than 2.3 km in the outer Oort Cloud (Weissman 1996) and assume a power index of $q = 3.5$, we will have $N_{D>900m} = 1.1 \times 10^{13}$ for the outer Oort Cloud. This number is about six orders lower than our upper limit estimate. If we consider there are five times more objects in the inner Oort Cloud, we have $N_{D>300m} = 8.2 \times 10^{14}$ for the inner Oort Cloud. This number is about three orders smaller than the upper limit we currently have. Although our upper limits are not stringent enough, they are the first obtained by observations. They also provide guidance for future observations of this kind.

5 SEARCH FOR OCCULTATIONS IN X-RAYS CAUSED BY SMALL TNOS IN THE FUTURE

To explore population properties of small bodies in the outskirt of our solar system, serendipitous occultation event search seems to be the only way. Count rates and data volume are the two major factors to consider.

For KBOs, since the Fresnel scale is about 30 m at 40 AU for 4-keV photons, one should look for occultation events at millisecond time scale. For a cetral-crossing event, if taking the relative speed between the observer and the TNO to be 30 km/s, the shortest shadow duration will be about 3 ms – recall that diffraction makes the shadow to be about 3.4 Fs for small occulting bodies. Search with 1-ms time bins is suggested for such a case. A count rate of about 4×10^4 cps will give 40 counts in a 1-ms bin, which is about enough for detecting occultation events. One may of course look for events caused by larger bodies with background sources of lower count rates, but that will probably require much larger data volume to have detection or to have meaningful upper limits to the size distribution, since the size distribution is generally believed to decrease quite fast towards the larger-size end. We estimated count rates of three X-ray space missions, ASTROSAT, Athena, and LOFT, for the nine compact X-ray sources, using detector response matrices provided by the instrumentation teams and typical source spectra reported in the literature. One can see that, in Table 3, Sco X-1 is still the only usable background source for all the three missions, GX5-1, Sco X-2 and Cyg X-1 are marginal ones for Athena, GX 5-1 is also marginal for ASTROSAT, and all the 9 sources can be used for LOFT. In our earlier efforts (Chang, Liu & Chen 2013), the obtained upper limit with several hundred kiloseconds data may be already quite close to the real distribution. We suggest that a few megaseconds data of these three missions with high enough count rates are likely to have some definite detections of such events.

As for Oort Cloud Objects, due to diffraction limit, one can only explore objects of sub-kilometer and kilometer size for inner and outer Oort Cloud Objects respectively. For this size range, light curves binned at 10 milliseconds are fine enough for occultation event search. It therefore only requires a lower count rate of about 4×10^3 cps to have 40 counts in one 10-ms bin. This why RXTE/PCA data of GX 5-1 can be used in this search but not in that for KBOs. All the nine sources can be used for ASTROSAT, Athena and LOFT for such search, except that Ser X-1 may be too dim for ASTROSAT. In this paper, however, we report upper limits, with about 1.6-Ms data, to the size distribution of inner and outer Oort Cloud Objects, which are three and six orders higher than the highest theoretical estimates in the literature. It does not seem feasible for these X-ray space missions to accumulate enough data volume to have definite detections, unless all the earlier theoretical works severely underestimate the number of Oort Cloud Objects.

On the other hand, it is relatively easier to accumulate a huge data volume in optical bands, see, e.g., the Miosotys (Shih et al. 2010), TAOS II (Lehner et al. 2014) and CHIMERA (Harding et al. 2016) projects. Because of longer wavelength, however, it can probe objects only down to size of 1 km, 10 km and 30 km or so for the Kuiper Belt, inner and outer Oort Cloud, respectively, again due to diffraction limit. It in turn requires even more data, say, about 300 times more compared with that in X-rays, depending on the actual size distribution. A major limiting factor for ground-based optical occultation survey is the finite angular sizes of the target stars, which are typically much larger than occulting bodies and the Fresnel scale in the Oort Cloud region. It does not help to have a smaller Fresnel scale by observing at shorter optical wavelength. Some detections have been reported with fewer data of high signal-to-noise ratio obtained by space missions like HST (Schlichting et al. 2012) and CoRoT (Liu et al. 2015). These high-quality data make possible the detection of occultation events caused by KBOs of about 500-m size, roughly half a Fresnel scale. It is probably much more difficult to detect occultation events by Oort Cloud Objects. A dedicated space mission with high quality data might be able to provide solutions.

ACKNOWLEDGMENTS

Comments from Matthew Lehner to improve this paper are very much appreciated. This research has made use of data obtained through the High Energy Astrophysics Science Archive Research Center Online Service, provided by

Sources	ASTROSAT/LAXPC (3-12 keV)	(12-80 keV)	Athena/WFI (0.2-2 keV)	(2-12 keV)	LOFT/LAD (2-12 keV)	Other names
4U 1758-25	1.5×10^4	—	9.9×10^2	1.5×10^4	2.3×10^5	1H1758-250, GX5-1
4U 1758-20	9.9×10^3	1.4×10^3	2.7×10^3	7.0×10^3	1.5×10^5	1H1758-205, GX9+1, Sgr X-3
4U 1617-15	1.5×10^5	1.2×10^4	5.3×10^5	2.6×10^5	3.0×10^6	1H1617-155, Sco X-1
4U 1813-14	7.4×10^3	—	1.6×10^3	7.7×10^3	1.2×10^5	1H1813-140, GX17+2, Ser X-2
4U 1702-36	9.5×10^3	—	4.5×10^3	1.0×10^4	1.5×10^5	1H1702-363, GX 349+2, Sco X-2
4U 1642-45	5.3×10^3	—	1.8×10^2	4.6×10^3	7.8×10^4	1H1642-455, GX340+0
4U 1837+04	2.8×10^3	—	6.1×10^3	3.5×10^3	4.9×10^4	1H1837+049, Ser X-1
4U 2142+38	5.8×10^3	—	4.5×10^3	8.0×10^3	1.0×10^5	1H2142+380, Cyg X-2
4U 1956+35	7.3×10^3	3.8×10^3	1.5×10^4	8.0×10^3	1.2×10^5	1H1956+350, Cyg X-1

Table 3. Estimated count rates, in units of count per second (cps), for some non-extended bright X-ray sources, which are potential background targets for serendipitous TNO occultation search in X-rays. All the nine listed sources are brighter than 0.1 Crab in all the 4th Uhuru (4U), HEAO 1 A-1 (A1), and RXTE All Sky Monitor (ASMquick) catalogues. The 4U catalog was compiled with observations conducted during 1972-1973, the A1 catalog was during 1977, and the ASMquick information is based on weekly average in August 2011. The estimated count rates are based on spectral models of each sources reported in the literature (Chang, Liu & Chen (2013), and references therein). LAXPC is the Large Area X-ray Proportional Counter on board ASTROSAT. WFI is the Wide Field Imager on board Athena. LAD is the Large Area Detector on board LOFT, whose count rate in this table is somewhat different from that in Chang, Liu & Chen (2013) because a more updated LOFT/LAD instrument response matrix (version 'M4') is used. For ASTROSAT/LAXPC, '—' indicates that the source count rate is below three times estimated background count rate. This list is sorted with the absolute value of their ecliptic latitude.

the NASA/Goddard Space Flight Center. This work was supported by the Ministry of Science and Technology of the Republic of China under grants 101-2923-M-007 -001 -MY3 and 102-2112-M-007 -023 -MY3.

REFERENCES

Ayre M., Bavdaz M., Ferreira I., Wille E., Lumb D., Linder M., 2015, Proceedings of the SPIE, Volume 9601, id. 96010L
Barnard R., Church M.J., Balucinska-Church M., 2003, A&A, 405, 237
Bickerton S. J., Kavelaars J. J., Welch D. L., 2008, AJ, 135, 1039
Bradshaw C.F., Geldzahler B.J., Fomalont E.B., 2003, ApJ, 592, 486
Brasser R., Morbidelli A., 2013, Icarus, 225, 40
Brasser R., Schwamb M. E., 2015, MNRAS, 446, 3788
Brown M. E., Trujillo C., Rabinowitz D., 2004, ApJ, 617, 645
Chang H.-K., King S.-K., Liang J.-S., Wu P.-S., Lin L.C.-C., Chiu J.-L., 2006, Nature, 442, 660
Chang H.-K., Liang J.-S., Liu C.-Y., King S.-K., 2007, MNRAS, 378, 1287
Chang H.-K., Liu C.-Y., Chen K.-T., 2011, MNRAS, 411, 427
Chang H.-K., Liu C.-Y., Chen K.-T., 2013, MNRAS, 429, 1626
Christian D. J., Swank J. H., 1997, ApJS, 109, 177
Chen Y.-T., Kavelaars J. J., Gwyn S., Ferrarese L., Côté P., Jordán A., Suc V., Cuillandre J.-C., Ip W.-H., 2013, ApJL, 775, L8
Dones L., Brasser R., Kaib N., Rickman H., 2015, Space Sci. Rev., 197, 191
Dones L., Weissman P. R., Levison H .F., Duncan M. J., 2004a, In: Star Formation in the Interstellar Medium, ed. D. Johnstone, F. C. Adams, D. N. C. Lin, D. A. Neufeld, & E. C. Ostriker (San Francisco), ASPC, 324, 371
Dones L., Weissman P. R., Levison H .F., Duncan M. J., 2004b, In: Comets II, ed. M. C. Festou, H. U. Keller, & H. A. Weaver (Univ. of Arizona Press, Tucson), pp. 153174.
Duncan M., Quinn T., Tremaine S., 1987, AJ, 94, 1330
Harding L. K., Hallinan G., Milburn J., Gardner P., Konidaris N., Singh N., Shao M., Sandhu J., Kyne G., Schlichting H. E., 2016, MNRAS, 457, 3036
Heisler J., 1990, Icarus, 88, 104
Hills J. G., 1981, AJ, 86, 1730
Hynes R. I., Schaefer B. E., Baum Z. A., Hsu C.-C., Cherry M. L., Scaringi S., 2016, MNRAS, 459, 3596
Jackson N. K., Church M. J., Balucińska-Church M., 2009, A&A,494, 1059
Kaib N. A., Quinn T., 2009, Science, 325, 1234
Lehner M. J., Wang S. Y., Alcock C. A., et al., 2014, Proceedings of SPIE, Volume 9145, id. 914513
Liu C.-Y., Chang H.-K., Liang J.-S., King S.-K., 2008, MNRAS, 388, L44
Liu C.-Y., Doressoundiram A., Roques F., Chang H.-K., Maquet L., Auvergne M., 2015, MNRAS, 446, 932
Nihei T.C., Lehner M.J., Bianco F.B., King S.-K., Giammarco J.M., Alcock C., 2007, AJ, 134, 1596
O'Brien D. P., Greenberg R., 2003, Icarus, 164, 334
Oort J. H., 1950, Bulletin of the Astronomical Institutes of the Netherlands, 11, 91
Revnivtsev M. G., Tsygankov S. S., Churazov E. M., Krivonos R. A., 2014, MNRAS, 445, 1205
Rickman H., 2014, Meteoritics & Planetary Science, 49, 8
Roques F. et al., 2006, AJ, 132, 819
Roques F. et al., 2009, EMP, 105, 201
Schlichting H. E. et al., 2012, ApJ, 761, 150
Shih I. C., Doressoundiram A., Boissel Y., Roques F., Dauny F., Felenbok P., Fernandez A., Guerin J., Chang H.-K., Liu C.-Y., 2010, Proceedings of the SPIE, Volume 7735, id. 773546
Singh K. P., et al., 2014, Proceedings of the SPIE, Volume

9144, id. 91441S
Sriram K., Choi C. S., Rao A. R., 2012, ApJS, 200, 16
Trujillo C. A., Sheppard S. S., 2014, Nature, 507, 471
Wang J.-H., et al., 2009, AJ, 138, 1893
Weissman P. R., 1996, In: Completing the Inventory of the Solar System, ed. T. W. Rettig & J. M. Hahn (San Francisco), ASPC, 107, 265
Yoshida F., Nakamura T., 2007, Planet. Space Sci., 55, 1113
Zane S., et al., 2014, Journal of Instrumentation, Volume 9, id. C12003
Zhang Z.-W. et al., 2013, AJ, 146, 14